iScience

Article

The role of Testis-Specific Protein Y-encoded-Like 2 in kidney injury

Mingxing Sui, Sijia Yan, Pei Zhang, ..., Yanfeng Li, Wenyu Zhao, Li Zeng

zwyisy@smmu.edu.cn (W.Z.)
shchyysyz@smmu.edu.cn (L.Z.)

Highlights

TSPYL2 was identified as a novel regulator of IRI-induced kidney damage

TSPYL2 promotes ACMSD transcriptional activation by regulating SREBP-2 acetylation

TSPYL2 regulates SREBP-2 acetylation by reducing SIRT1 and increasing p300 protein

Article

The role of Testis-Specific Protein Y-encoded-Like 2 in kidney injury

Mingxing Sui,[1,3] Sijia Yan,[2,3] Pei Zhang,[1,3] Yuhong Li,[1] Kewen Chen,[1] Yanhua Li,[1] Hanlan Lu,[1] Yanfeng Li,[1] Wenyu Zhao,[1,*] and Li Zeng[1,4,*]

SUMMARY

Renal ischemia-reperfusion injury (IRI) is a major cause of acute kidney injury (AKI). Recent findings suggest that Testis-Specific Protein Y-encoded-Like 2 (TSPYL2) plays a fibrogenic role in diabetes-associated renal injury. However, the role of TSPYL2 in IRI-induced kidney damage is not entirely clear. In this study, we found that the expression of TSPYL2 was upregulated in a mouse model of AKI and in the hypoxia/reoxygenation (H/R) cell model. Knockdown of TSPYL2 attenuated kidney injury after IRI. More specifically, the knockdown of TSPYL2 or aminocarboxymuconate-semialdehyde decarboxylase (ACMSD) alleviated renal IRI-induced mitochondrial dysfunction and oxidative stress *in vitro* and *in vivo*. Further investigation showed that TSPYL2 regulated SREBP-2 acetylation by inhibiting SIRT1 and promoting p300 activity, thereby promoting the transcriptional activity of ACMSD. In conclusion, TSPYL2 was identified as a pivotal regulator of IRI-induced kidney damage by activating ACMSD, which may lead to NAD+ content and the damaging response in the kidney.

INTRODUCTION

Acute kidney injury (AKI) is a common condition and affects approximately ~15% of adults and 25% of children who are hospitalized.[1,2] It is associated with a higher risk of chronic kidney disease (CKD), transition from pre-existing CKD to end-stage renal disease and increased risk of death.[1,3–5] Unfortunately, there are no definite therapies available for the treatment of hospital-acquired AKI.

AKI originates from multiple causes, and a common cause is renal ischemia-reperfusion injury (IRI), which often occurs in the context of multiple organ failure, sepsis, and vascular occlusion.[6] Ischemia-reperfusion is characterized by a restricted blood flow leading to temporary deficiency of oxygen and followed by a quick restoration of oxygen supply. IRI in the kidneys may lead to mitochondrial damage in renal tubular cells, as shown by decreased mitochondrial abundance, swelling, and disruption of cristae.[7,8] Disruption of mitochondria leads to release of reactive oxygen species (ROS) and mitochondrial DNA (mtDNA), which may be signals for cell apoptosis and proinflammation, respectively.[9] Indeed, oxidative stress, insufficient production of ATP, renal cell apoptosis and necrosis, and inflammation follow IRI.[10–12] The complex mechanisms and mediators that are involved in mitochondrial dysfunction after IRI in the kidneys are largely unknown, and therefore there are no available therapies that target the reduction of mitochondrial damage in the injured kidneys. A better understanding of the regulators of the pathophysiological processes underlying kidney injury may result in the development of targeted therapies to prevent AKI.

The family of testis-specific protein, Y-encoded (TSPY) belongs to the nucleosome assembly protein (NAP) superfamily that is characterized by a NAP domain for nucleosome remodeling and gene expression regulation.[13] TSPY was found to interact with cyclin B and enhance cyclin B-CDK1 phosphorylation leading to increased cell proliferation. Later, TSPY-like 2 (TSPYL2, also known as DENTT, CDA1 and TSPX) was discovered to play an opposite role in cell cycle control; TSPYL2 inhibits cyclin B-CDK1 activity.[14] Experiments with TSPYL2 deficient mice showed that TSPYL2 is important for G1 checkpoint maintenance under stress conditions.[15] It is therefore suggested that TSPYL2 has a tumor suppressor role and important functions in cell growth and DNA damage response regulation.

DNA damage has been implicated in both acute and chronic kidney injury. In the kidney, DNA damage can affect the local microenvironment by triggering a damage response and cell proliferation to replenish injured cells, and inducing systemic responses to reduce exposure to stress.[16] Kishi et al. proved that following kidney epithelial cell injury, DNA damage repair plays the pivotal role in recovery and longevity via reducing apoptosis, cell-cycle arrest, and fibrosis.[17] Recent findings suggest for TSPYL2 has important functions in DNA damage response regulation and kidney injury repair. A more recent study found that upon DNA damage, TSPYL2 regulates silent mating type information regulation 2 homolog 1 (SIRT1) and p300 and thereby stimulates p53-dependent cell death.[18] These findings suggests that the accumulation of TSPYL2 contributes to the regulation of apoptosis. Interestingly, the authors of this study noted that the role

of TSPYL2 in the regulation of apoptosis is not specific for the cells that were used in the experiments. A previous study revealed that the renal expression of CDA1, a phosphorylated protein encoded by TSPYL2, was increased in diabetic nephropathy (DN) and the gene deletion of CDA1 hindered diabetes-associated renal injury and ECM accumulation.[19] However, the role of TSPYL2 in IRI-induced kidney damage is not entirely clear.

It was hypothesized that TSPYL2 may play a role in the mitochondrial dysfunction and oxidative stress following IRI in the kidneys. Therefore, the aim of this study was to investigate the role of TSPYL2 in kidney IRI and to further explore the signaling pathway downstream of TSPYL2 that leads to damage and eventually cell death. To this end, a mouse model of IRI was generated and used for experiments in combination with a cell model of hypoxia/reoxygenation (H/R) injury.

RESULTS

Upregulated testis-specific protein Y-encoded-like 2 expression in the animal model of acute kidney injury and in the hypoxia/reoxygenation cell model

To investigate whether TSPYL2 is upregulated in response to reperfusion, mice of the IRI mouse model were exposed to ischemia and reperfusion was performed for 6, 12, and 24 h. Compared to mice without exposure to ischemia and reperfusion (sham), TSPYL2 mRNA levels were increased in the kidneys of ischemia mice exposed to reperfusion. TSPYL2 mRNA levels significantly increased more with longer reperfusion time (Figure 1A). A similar pattern was seen for TSPYL2 protein expression (Figure 1B). Immunofluorescence staining of ischemic kidneys of mice exposed to reperfusion showed increased staining for TSPYL2 compared to sham mice. A higher number of TSPYL2-positive cells was seen with longer perfusion time (Figures 1C and 1D).

When HK-2 cells were used for experiments, time-dependent upregulated TSPYL2 protein expression was observed when hypoxic cells were exposed to 2, 4 or 6 h of reoxygenation compared to normoxic cells (control) (Figure 1E). These data suggested that the upregulation of TSPYL2 might be related to renal injury after IRI.

Knockdown of testis-specific protein Y-encoded-like 2 in mice attenuates kidney injury after ischemia-reperfusion injury

Two days before IRI, mice were injected with shTSPYL2 plasmid to reduce the expression of TSPYL2 protein and samples for analyses were collected at 24 h (Figure 2A). Western blot analysis confirmed the downregulation of TSPYL2 protein levels in the kidneys of mice injected with shTSPYL2 compared to mice injected with shControl (Figure 2B). When mice were exposed to IRI, TSPYL2 protein levels were strongly upregulated in the kidneys of shControl mice, but only a small increase in TSPYL2 protein expression was seen in shTSPYL2 mice (Figure 2B). These findings were confirmed by the immunofluorescence staining of TSPYL2 in the kidneys of mice (Figure 2C).

To survey the effect of the knockdown of TSPYL2 on renal function in mice after IRI, the levels of serum creatinine (Scr), blood urea nitrogen (BUN), and KIM-1 were detected. The results showed that the levels of Scr, BUN and KIM-1 were upregulated after IRI compared to the sham procedure, which indicated abnormal renal function, but the increase was lower in shTSPYL2 mice than in the shControl mice (Figures 2D–2F). Finally, the morphology of the kidneys assessed by H&E stainings demonstrated similar patterns with low kidney scores for sham mice and higher scores for IRI-treated mice. In the IRI-exposed mice, the kidney injury score was lower though in the shTSPYL2 mice than in the shControl mice (Figures 2G and 2H).

Knockdown of testis-specific protein Y-encoded-like 2 in mice reduces ischemia-reperfusion injury-induced apoptosis and oxidative stress

After establishing that TSPYL2 is involved in kidney injury after IRI, the role of TSPYL2 in this process was further explored. Two measurements of apoptosis, TUNEL staining and expression of cleaved caspase-3, were examined in the kidneys of shControl and shTSPYL2 mice under sham or IRI conditions. After IRI, TUNEL staining was significantly increased in shControl mice compared to sham-treated mice, but lower in shTSPYL2 mice (Figure 3A). A similar pattern was seen for cleaved caspase-3; staining was significantly increased in shControl mice after IRI compared to sham conditions with a lower increase in shTSPYL2 mice after IRI (Figure 3B).

Further investigation of the pro-apoptotic protein Bax and the anti-apoptotic protein Bcl-2 by Western blot analyses of kidney tissues was done. After IRI exposure, Bax levels were increased in shControl mice and to a lesser degree increased in shTSPYL2 mice. In contrast, levels of Bcl-2 decreased in shControl mice after IRI and returned to similar levels as those of sham-treated mice in shTSPYL2 mice after IRI. Also, levels of cleaved caspase-3 as a marker of apoptosis were investigated by Western blotting and showed similar patterns as the pro-apoptotic protein Bax (Figure 3C).

To determine the effect of TSPYL2 on oxidative stress, the accumulation of reactive oxygen species (ROS) was measured in the kidneys of mice. Flow cytometry showed increased levels of ROS in IRI-exposed shControl mice compared to sham mice. However, the levels of ROS were reduced in IRI-exposed shTSPYL2 mice when compared to IRI-exposed shControl mice (Figure 3D). Also, levels of markers of oxidative stress (MDA) and antioxidants (GSH and SOD) were measured by ELISA. Compared to sham mice, MDA was upregulated in IRI-treated shControl mice and returned in IRI-treated shTSPYL2 mice (Figure 3E). The opposite pattern was observed for the antioxidants GSH and SOD; levels of GSH and SOD were decreased in IRI-exposed shControl mice when compared to sham-treated mice and levels in IRI-exposed shTSPYL2 mice increased to similar levels as those in sham-treated mice (Figures 3F and 3G). These data suggested that TSPYL2 knockdown might attenuate renal IRI by alleviating apoptosis and oxidative stress.
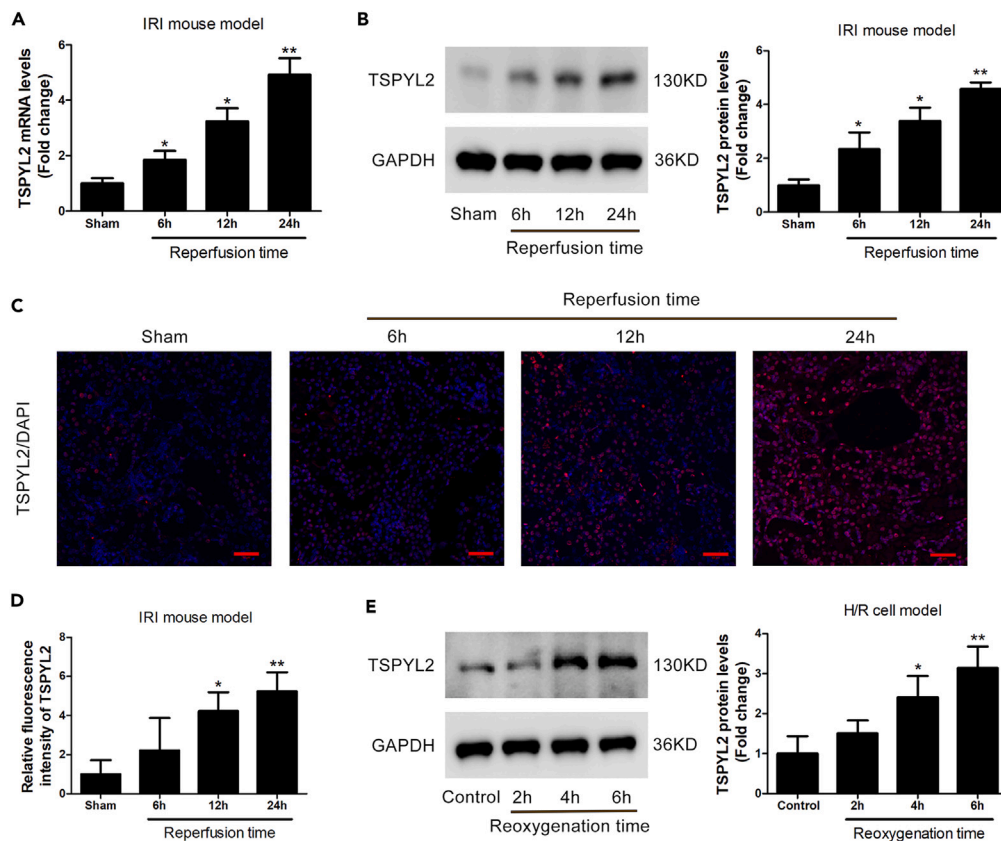
Figure 1. Expression of TSPYL2 is induced in the animal model of acute kidney injury (AKI) and in an H/R cell model

(A) Renal TSPYL2 mRNA levels were measured by quantitative real-time RT-PCR in sham-treated mice and ischemic mice exposed to reperfusion after 6h, 12h, or 24 h.

(B) TSPYL2 protein levels in the kidneys were detected by Western blot analysis in sham-treated and ischemic mice after different reperfusion times. Levels of GADH were used as loading control. A representative blot is shown and a bar graph of multiple experiments.

(C and D) Kidney sections of sham-treated or ischemic mice with reperfusion after 6h, 12h, or 24h were stained immunohistochemically with specific antibodies against TSPYL2 and DAPI. (C) Representative images indicate TSPYL2 protein expression in red and DAPI in blue. Bar = 50 μm. (D) Bar graph shows the average of several experiments of the percentage TSPYL2-positive cells relative to the sham group.

(E) TSPYL2 protein levels in HK-2 cells were detected by Western blot analysis in control cells and in hypoxia-treated cells with reoxygenation after 2h, 4h, or 6h. GAPDH was used as a loading control. A representative blot is shown and a bar graph of TSPYL2 expression relative to sham group from three independent experiments. Data are represented as mean ± SD (n = 3–6). p value calculated was determined by a two-tailed unpaired Student's t test. *p < 0.05, **p < 0.01 versus sham mice or control cells.

Knockdown of testis-specific protein Y-encoded-like 2 in mice attenuates NAD^{+} loss and decreases aminocarboxymuconate-semialdehyde decarboxylase expression after ischemia-reperfusion injury

Homeostasis of NAD+ is important for renal health and it has been described that decreased levels of NAD+ impair energy generation after AKI.[20] To investigate the role of TSPYL2 on NAD+, levels of NAD+ and NADH in the kidneys of mice were measured. After IRI in the renal cortex, NAD+ levels were decreased in shControl mice compared to sham-treated mice, whereas NAD+ levels in shTSPYL2 mice were similar as those in sham-treated mice (Figure 4A). Levels of NADH were decreased in IRI-treated shControl and IRI-treated shTSPYL2 mice compared to sham-treated mice (Figure 4B), but the ratio of NAD+/NADH in IRI-treated shControl mice was not different than in sham-treated mice and the ratio in IRI-treated shTSPYL2 mice was higher than in IRI-treated shControl mice (Figure 4C).

An important regulator of NAD+ metabolism is alpha-amino-beta-carboxy-muconate-semialdehyde decarboxylase (ACMSD)[21] and mRNA and protein levels of ACMSD were investigated in the kidneys of mice after IRI. Staining for ACMSD was significantly increased in shControl mice after IRI when compared to sham mice. When compared to IRI-treated shControl mice, the percentage of ACMSD-positive cells was decreased in IRI-treated shTSPYL2 mice (Figure 4D). A similar pattern was observed when examining ACMSD protein levels by Western blotting; increased levels of ACMSD in IRI-treated shControl mice compared to sham-treated mice and reduced levels in IRI-treated shTSPYL2 mice compared to IRI-treated shControl mice (Figure 4E). Finally, these findings were confirmed by analysis of mRNA levels of ACMSD (Figure 4F). These results indicated that TSPYL2 and ACMSD
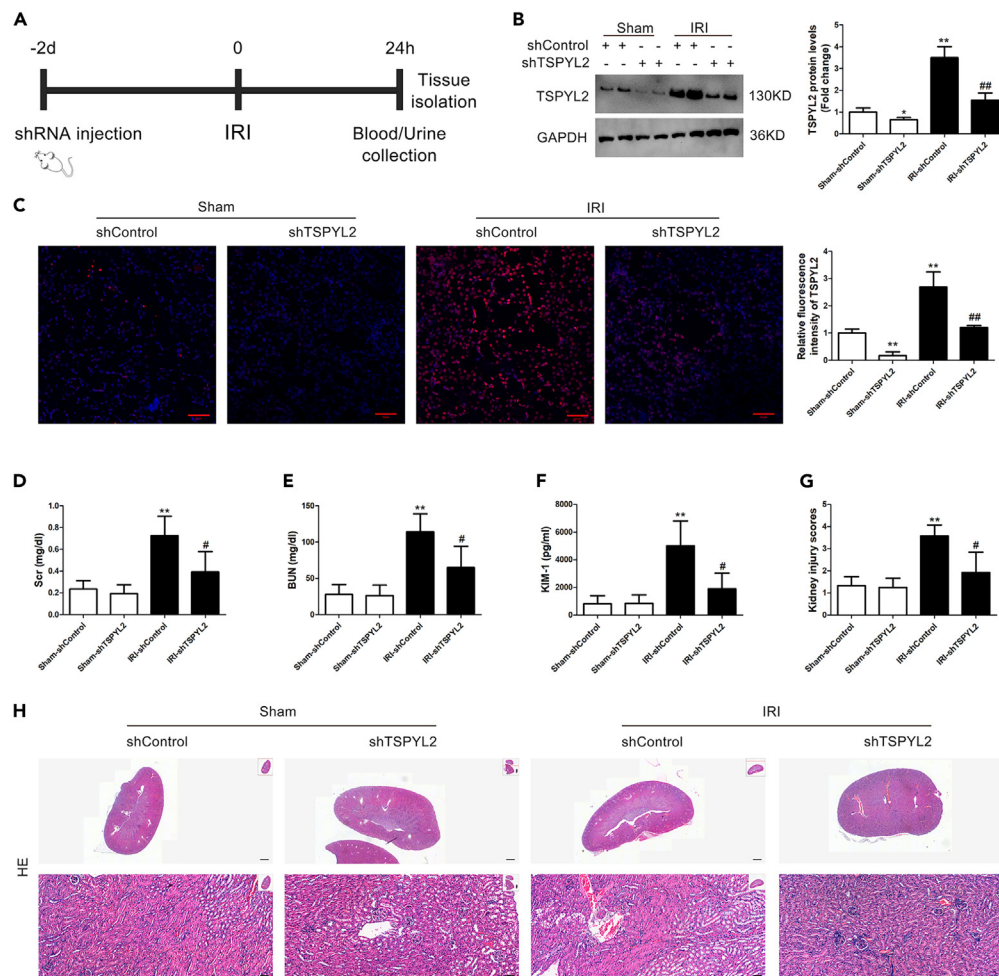
Figure 2. Knockdown of TSPYL2 attenuated kidney injury after ischemic-reperfusion injury (IRI)

(A) Experimental design. Injection of a short hairpin RNA plasmid in mice was done two days before exposure to IRI. After 24h, blood and urine were collected, and tissue was isolated.

(B) A representative Western blot of renal TSPYL2 protein expression in mice groups as indicated, with GAPDH as a loading control. The two lanes in the same group represent two samples from two different mice. In addition, a bar graph of several experiments showing TSPYL2 expression relative to the sham-shControl group (n = 6).

(C) Representative images show renal TSPYL2 expression in red and DAPI in blue in mice. Quantitative analyses of several experiments of the TSPYL2-positive area for four mice groups as indicated. At least five randomly selected fields were evaluated per mice. Bar = 50 μm.

(D) The level of Scr was determined for the four mice groups as indicated.

(E) BUN levels were measured in mice as indicated.

(F) Injury in kidney proximal tubular cells in mice was evaluated by measuring the concentration of urinary Kim-1.

(G) Kidney sections of mice were subjected to H&E staining. A bar graph with quantitative analyses of injured tubules assessed by kidney injury score is shown for the four groups as indicated.

(H) Representative images of H&E stainings of mice. Images in the right upper corner are enlarged and presented in the larger images. Upper panels, bar = 700 μm; lower panels, bar = 50 μm. Data are represented as mean ± SD (n = 4–6). p value calculated was determined by a two-tailed unpaired Student's t test. $*p < 0.05$, $**p < 0.01$ versus sham-shControl mice; $\#p < 0.05$, $\#\#p < 0.01$ versus IRI-shControl mice.

both regulate NAD and that TSPYL2 regulates the protein levels of ACMSD, which may be involved in the development of kidney injury after IRI.

Knockdown of testis-specific protein Y-encoded-like 2 or aminocarboxymuconate-semialdehyde decarboxylase in HK-2 cells ameliorates mitochondrial dysfunction, oxidative stress and apoptosis induced by hypoxia/reoxygenation injury

HK-2 cells exposed to H/R injury were used as an *in vitro* model of AKI to further investigate the role of TSPYL2 and ACMSD in this process. Knockdown of TSPYL2 or ACMSD in HK-2 cells by transfection with siRNA against TSPYL2 or ACSMD was confirmed by reduced
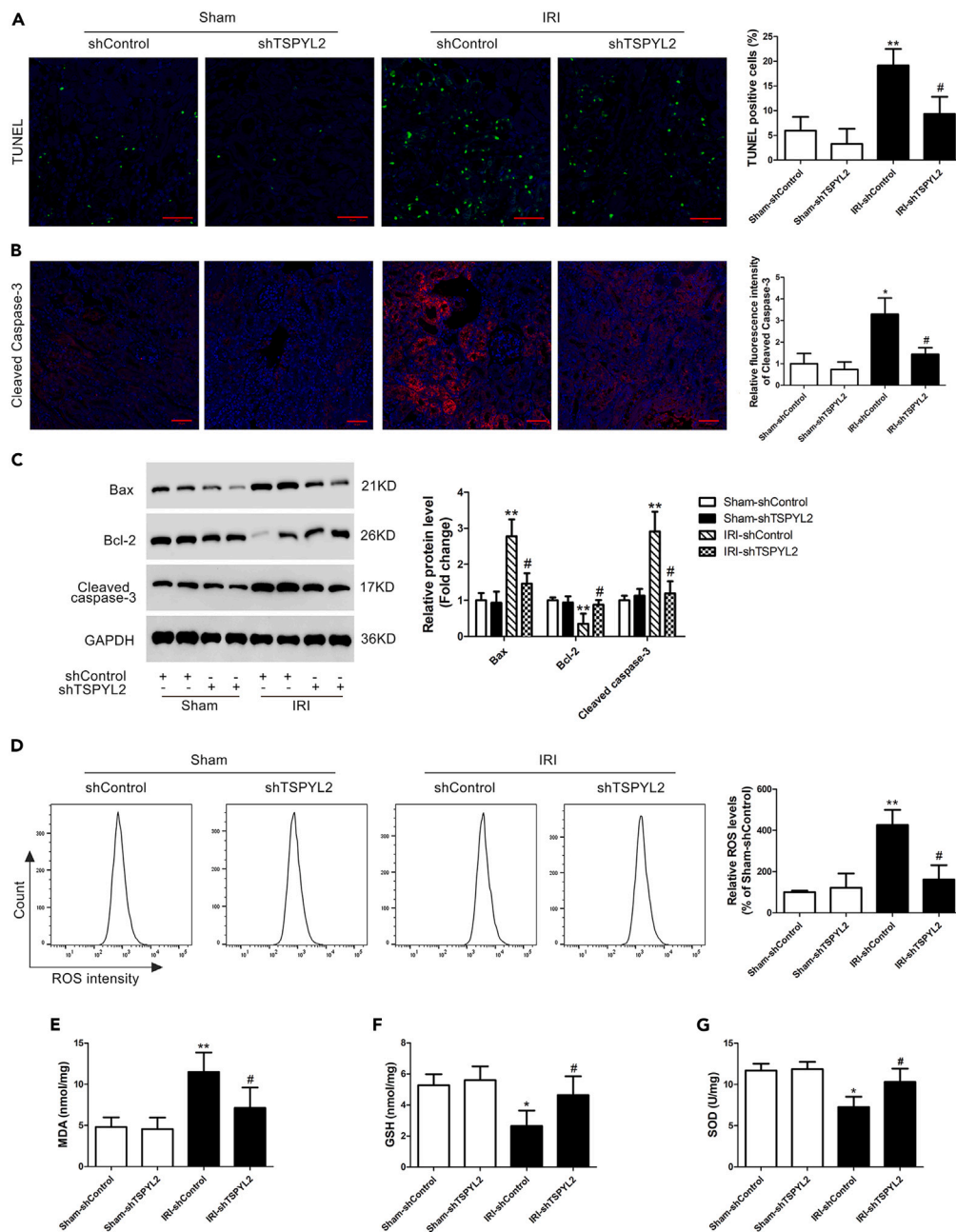
Figure 3. Knockdown of TSPYL2 inhibited IR-induced apoptosis and oxidative stress in the kidney *in vivo*

(A) Representative images show TUNEL-positive cells in green in the kidneys of mice and the bar graph depicts the percentage of TUNEL-positive cells. Bar = 50 μm.

(B) Representative images show cleaved caspase 3 staining in red and DAPI in blue in the kidneys of mice as indicated. The bar graph shows the percentage of caspase 3-positive cells. Bar = 50μm.

(C) Representative Western blots show the renal expression of Bax, Bcl-2, and cleaved caspase 3 in mice as indicated. GADPH was used as a loading control. The two lanes in same group represent two samples from two different mice. Quantitative analyses of Western blots of several experiments for the renal expression of Bax, Bcl-2, and cleaved caspase 3 in mice (n = 6).

(D) Representative flow cytometry plots of ROS staining in renal tissues of mice and quantitative analysis of several experiments of renal ROS levels in each group relative to the sham-shControl group.

(E–G) ELISA assays were used to measure the concentration of MDA, GSH and SOD in the kidney of mice. Data are represented as mean $\pm$ SD (n = 4–6). p value calculated was determined by a two-tailed unpaired Student's t test. *$p < 0.05$, **$p < 0.01$ versus sham-shControl mice; #$p < 0.05$ versus IRI-shControl mice.
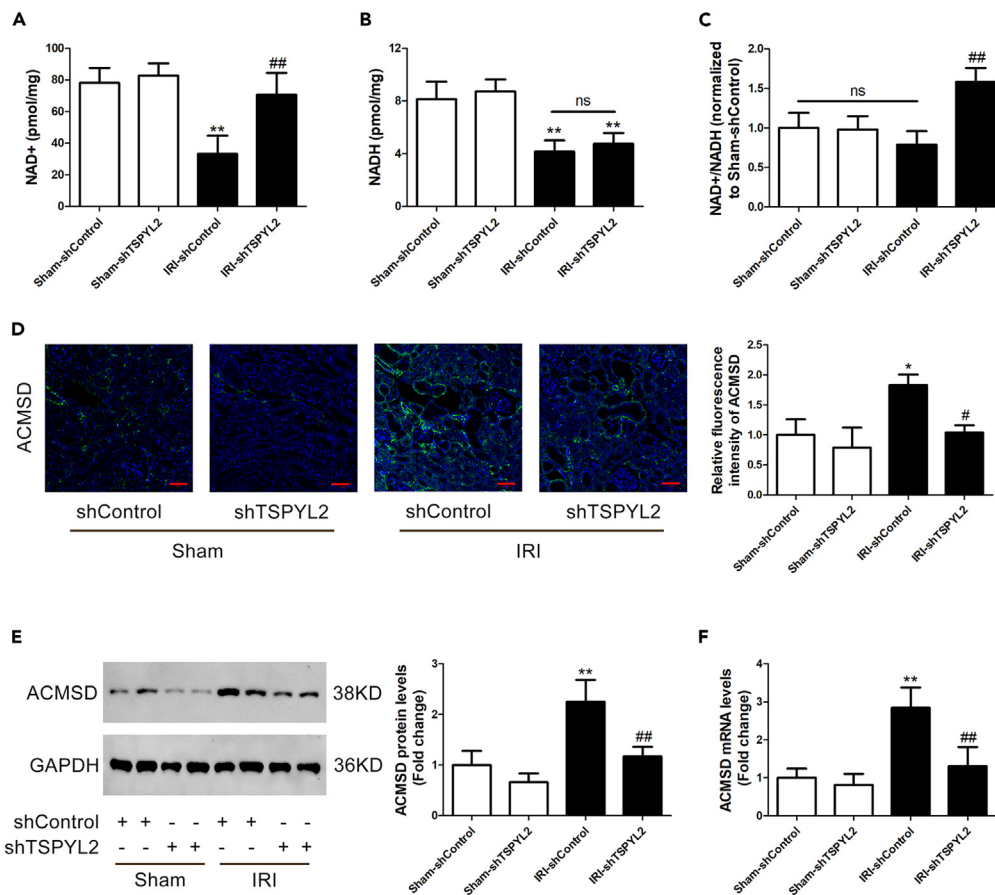
Figure 4. Knockdown of TSPYL2 attenuates NAD+ loss and decreases ACMSD expression after IRI

(A) Renal NAD+ levels were measured in mice.

(B) NADH measurements were performed in the kidneys of mice.

(C) The ratio of NAD$^+$/NADH was analyzed and expressed relative to that of the sham-shControl group.

(D) Representative images show renal ACMSD staining in blue in mice as indicated. Bar = 50 μm. The bar graph shows the average of quantitative analyses of several experiments of the percentage ACMSD-positive area in the kidneys for the four mice groups as indicated.

(E) A representative Western blot of renal ACMSD protein expression is shown for mice as indicated. The same mice are tested in Western blot of ACMSD and TSPYL2 protein. The bar graph shows renal ACMSD protein expression relative to the sham-shControl group.

(F) ACMSD mRNA levels in the kidneys of mice were determined for the four groups. Data are represented as mean ± SD (n = 4–6). p value calculated was determined by a two-tailed unpaired Student's t test. *p < 0.05, **p < 0.01 versus sham-shControl group; #p < 0.05, ##p < 0.01 versus IRI-shControl group, "ns" means not statistically different.

levels of TSPYL2 and ACMSD when compared to high levels of these proteins in HK-2 cells transfected with siControl (Figure 5A). After H/R injury, the silencing of TSPYL2 can reduced ACMSD levels but silenced ACMSD cannot reduced TSPYL2 levels in HK-2 cells (Figure 5A).

Cell viability as measured by CCK8 was reduced in HK-2 cells transfected with siControl and exposed to H/R injury but returned to normal in H/R-exposed cells transfected with siTSPYL2 and siACMSD (Figure 5B). Cell apoptosis measured by TUNEL staining. In HK-2 cells after H/R injury, cell apoptosis was reduced in both siTSPYL2 and siACMSD cells compared to siControl cells (Figures 5C and 5D). Again, protein levels of pro- or anti-apoptotic markers Bax, Bcl-2, and cleaved caspase-3 were determined by Western blotting, but this time in HK-2 cells. Protein levels of the pro-apoptotic marker Bax and cleaved caspase-3 were significantly increased after H/R injury in siControl cells compared to control HK-2 cells (no H/R injury). Interestingly, after H/R injury, levels of Bax and cleaved caspase-3 were reduced in siTSPYL2 and siACMSD cells compared to siControl cells. The opposite pattern was observed for the anti-apoptotic marker Bcl-2 (Figure 5E). Subsequently, levels of NAD+ were measured and showed decreased levels in HK-2 cells exposed to H/K injury and transfected with siControl compared to control HK-2 cells. Levels of NAD+ were restored though in HK-2 cells exposed to H/R injury and transfected with siTSPYL2 or siACMSD (Figure 5F).

Other markers of mitochondrial function -mitochondrial DNA copy number, and ATP production-confirmed earlier findings; levels were lower in HK-2 cells exposed to H/R injury and transfected with siControl and levels restored to normal in cells exposed to H/R injury and transfected with siTSPYL2 or siACMSD (Figures 5G and 5H).
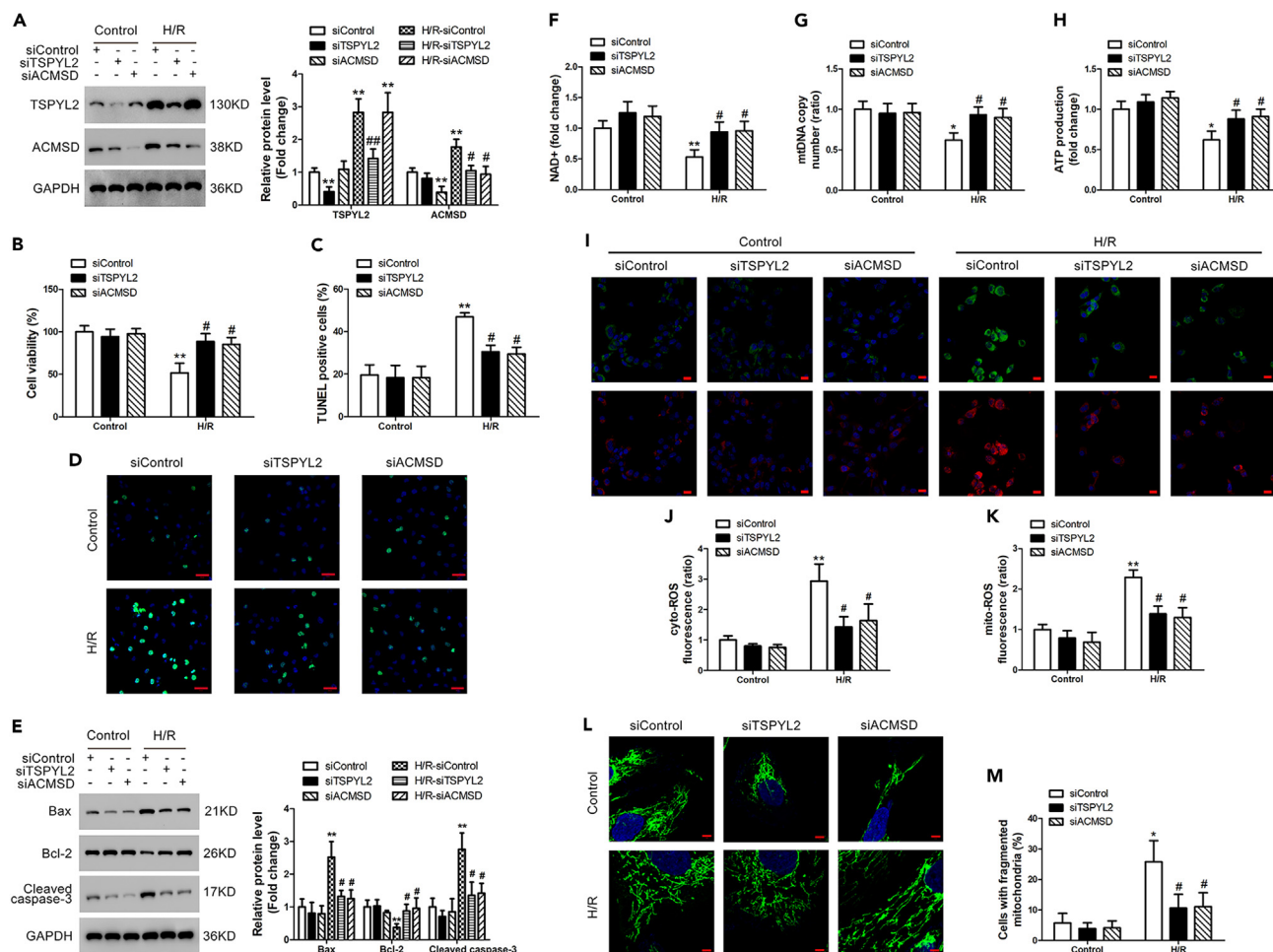
Figure 5. Knockdown of TSPYL2 or ACSMD ameliorated mitochondrial dysfunction, oxidative stress, and apoptosis induced by hypoxia-reoxygenation (H/R) injury in HK-2 cells

(A) HK-2 cells were transfected with siTSPYL2 or siACSMD or a negative control (siControl) 24h before exposure to H/R or no exposure (Control). Representative Western blots for the expression of TSPYL2 and ACSMD are shown. GAPDH was used as a loading control. The bar graphs show the quantification of Western blots for TSPYL2 and ACSMD of three independent experiments.

(B) Cell viability of HK-2 cells was detected using the CCK8 assay in the indicated groups.

(C and D) Apoptosis of HK-2 cells was measured by TUNEL assay. Bar = 50 μm. The bar graph shows the percentage of TUNEL apoptotic cells.

(E) Representative Western blots of staining for Bax, Bcl-2, and cleaved caspase-3 in HK-2 cells are shown. GADPH was used as a loading control. Bar graphs show the results of Bax, Bcl-2, and cleaved caspase-3 levels in HK-2 cells from three independent experiments.

(F) NAD$^+$ levels in HK-2 cells were measured.

(G) mtDNA copy number in HK-2 cells was determined by analysis of the ND1 segment-18S segment ratio using qPCR.

(H) Cellular ATP production was measured in HK-2 cells.

(I) Staining of cytoplasmic ROS (cyto-ROS) in green and mitochondrial ROS (mito-ROS) in red in HK-2 cells was performed using CellROX green reagent and MitoSOX red reagent, respectively. Bar = 20 μm.

(J and K) Bar graphs showing relative fluorescence levels of cyto-ROS (J) and mito-ROS (K) are shown.

(L) Representative images of mitochondrial divisions in HK-2 cells are shown by the immunohistochemical staining of mitochondria in green. Bar = 5 μm.

(M) Mitochondrial fission was quantified in HK-2 cells by counting the percentage of cells with fragmented mitochondria. Data are represented as mean ± SD (n = 3). p value calculated was determined by a two-tailed unpaired Student's t test. *$p < 0.05$, **$p < 0.01$ versus Control-shControl group; #$p < 0.05$, ##$p < 0.01$ versus H/R-shControl group.

Immunohistochemical studies to investigate oxidative stress showed increased levels of cytoplasmic and mitochondrial ROS in siControl HK-2 cells after H/R injury when compared to control HK-2 cells and decreased levels in siTSPYL2 and siACMSD HK-2 cells after H/R injury when compared to siControl cells after H/R injury (Figures 5I–5K). When looking at cells with fragmented mitochondria by immunohistochemical staining, the percentage of cells with fragmented mitochondria was increased after H/R injury in siControl cells when compared to control cells, whereas the percentage of cells decreased in siTSPYL2 and siACMSD cells after H/R injury when compared to siControl cells after H/R

injury (Figures 5L and 5M). Taken together, these data suggest that TSPYL2 and ACMSD can regulate cell apoptosis, oxidative stress, and mitochondrial dysfunction, which ameliorate H/R-induced cell injury in HK-2 cells.

Aminocarboxymuconate-semialdehyde decarboxylase overexpression aggravates mitochondrial dysfunction, oxidative stress, and apoptosis induced by hypoxia/reoxygenation injury in testis-specific protein Y-encoded-like 2-knockdown HK-2 cells

To investigate whether ACMSD plays a pivotal role in TSPYL2-mediated AKI, ACMSD was overexpressed with a plasmid carrying the human ACMSD in HK-2 cells transfected with siControl or siTSPYL2 expose to H/R after 24 h. Overexpression of ACMSD in control and H/R-treated cells was confirmed by Western blotting (Figure 6B). Results showed that H/R injury induces the expression of ACMSD, which was decreased in H/R-treated siTSPYL2+MOCK cells and upregulated again in H/R-treated siTSPYL2 + ACSMD cells. But the TSPYL2 levels are not affected by the overexpression of ACMSD (Figure 6A). After H/R injury or overexpression of ACMSD, cell viability as measured by CCK8 was decreased, returned to normal in H/R-treated siTSPYL2+MOCK cells, further decreased in H/R-treated siControl+ACSMD cells and cell viability in H/R-treated siTSPYL2 + ACSMD cells returned to similar levels as those in H/R-treated siControl+MOCK cells (Figure 6B).

Subsequently, apoptosis measured by TUNEL staining and markers of pro-apoptosis and anti-apoptosis measured by Western blotting were investigated in HK-2 cells. Percentage of apoptotic cells measured by TUNEL staining was increased after H/R injury or overexpression of ACMSD, reduced after H/R injury in siTSPYL2+MOCK cells, further increased by the overexpression of ACMSD after H/R injury and levels in H/R-treated siTSPYL2 + ACSMD cells were similar as those in H/R-treated siControl+MOCK cells (Figure 6C). A similar pattern was observed for Bax and cleaved caspase-3, and the opposite pattern for Bcl-2 (Figure 6D). These data indicate that TSPYL2 regulate H/R-induced apoptosis via ACMSD in HK-2 cells.

Furthermore, levels of NAD+, copy number of mitochondrial DNA and ATP levels were examined in H/R injury-exposed HK-2 cells with the transfection of siControl or siTSPYL2 plus MOCK or ACMSD plasmids. The same pattern was observed for these markers: H/R injury or over-expression of ACMSD reduced levels of NAD+, copy number of mDNA, and ATP levels, and these restored to normal in H/R-treated siTSPYL2+MOCK cells and were reduced again in H/R-treated siTSPYL2 + ACSMD cells, further reduced in H/R-treated siControl+ACSMD cells (Figures 6E–6G). Cytoplasmic ROS, mitochondrial ROS (Figures 6H–6J) and percentage of cells with fragmented mitochondria (Figures 6K and 6L) as markers of mitochondrial dysfunction were increased after H/R injury or overexpression of ACMSD, reduced after H/R injury in siTSPYL2+MOCK cells and increased again after H/R injury in siTSPYL2 + ACSMD cells, further increased in H/R-treated siControl+ACSMD cells (Figures 6H–6L). These results indicate that TSPYL2 regulate H/R-induced oxidative stress and mitochondrial dysfunction via ACMSD in HK-2 cells.

Testis-specific protein Y-encoded-like 2 promotes aminocarboxymuconate-semialdehyde decarboxylase transcriptional activation by regulating SREBP-2 acetylation

It is unknown whether ACMSD is downstream in the pathway of TSPYL2 in the kidney and if so, how TSPYL2 affects ACMSD. Therefore, several experiments were undertaken to examine these questions.

First, HK-2 cells exposed to H/R injury showed increased mRNA levels of ACMSD, which was significantly decreased in siTSPYL2 cells after H/R injury, indicating that knockdown of TSPYL2 downregulates ACSMD expression (Figure 7A).

To examine which protein may mediate the regulation of ACMSD by TSPYL2, the JASPAR database was searched and indicated a binding site for SREPB-2 on the ACMSD promotor 855 to 865 bp from the ACMSD transcription start site (Figure 7B). Subsequently, luciferase reporter analysis was performed to investigate whether SREBP-2 indeed transactivates the ACMSD promoter. In wild-type HK-2 cells, transfection of siTSPYL2 reduced luciferase activity, transfection with the plasmid carrying SREBP-2 increased luciferase activity and eliminate the inhibition effect of siTSPYL2, whereas there was no difference in luciferase activity in HK-2 cells with mutant ACMSD promotor regions (Figure 7C). This indicates that TSPYL2 regulates the ACMSD promoter activity via SREBP-2. To confirm that SREBP-2 binds to the ACMSD promoter under H/R injury conditions, HK-2 cells were left untreated or exposed to H/R injury and collected for ChIP assays. Immunoprecipitation was done with anti-SREBP-2 antibody and levels of ACMSD promoter that were present in samples were normalized to levels of IgG immunoprecipitation in the untreated HK-2 cells with siControl transfection. Compared to untreated HK-2 cells (no H/R injury), level of ACMSD promotor was increased in H/R injury-treated siControl cells, whereas this was decreased in H/R injury-treated siTSPYL2 cells (Figure 7D). This indicates that TSPYL2 mediates SREBP-2 binding to the promoter of ACMSD (Figure 7D).

Indeed, in the IRI mouse model, mice exposed to IRI showed increased levels of SREBP-2 in the kidneys, while this was decreased in IRI-treated shTSPYL2 mice (Figure 7E). Other mediators that on their turn play role in the downstream signaling of TSPYL2 to SREBP-2 may be SIRT1 and p300. These proteins were examined in the IRI mouse model and Western blotting showed reduced levels of SIRT1 in mice exposed to IRI, whereas levels returned to normal in shTSPYL2 mice after IRI injury. In contrast, p300 levels were increased in mice after IRI, and reduced in shTSPYL2 mice after IRI (Figure 7E). These findings were confirmed by experiments with HK-2 cells (Figure 7F).

To test the hypothesis that TSPYL2 signaling resulted in the acetylation of SREBP-2, immunoprecipitation of SREBP-2 in the kidneys of mice exposed to IRI were performed and precipitates were stained for acetylation. Indeed, IRI exposure resulted in the acetylation of SREBP-2, which was reduced in shTSPYL2 mice compared to the shControl mice (Figure 7G). Experiments were repeated in HK-2 cells and the *in vivo* findings were confirmed *in vitro* (Figure 7H). When in addition to transfection with TSPYL2, HK-2 cells were transfected with plasmid carrying p300 or siSIRT1,the expression of p300 and SIRT1 was confirmed by Western blotting (Figure 7I), these cells showed similar levels of SREBP-2 acetylation after H/R injury as in H/R-treated cells, and the effect of TSPYL2 was abolished by the overexpression of p300 or siSIRT1 (Figure 7J).
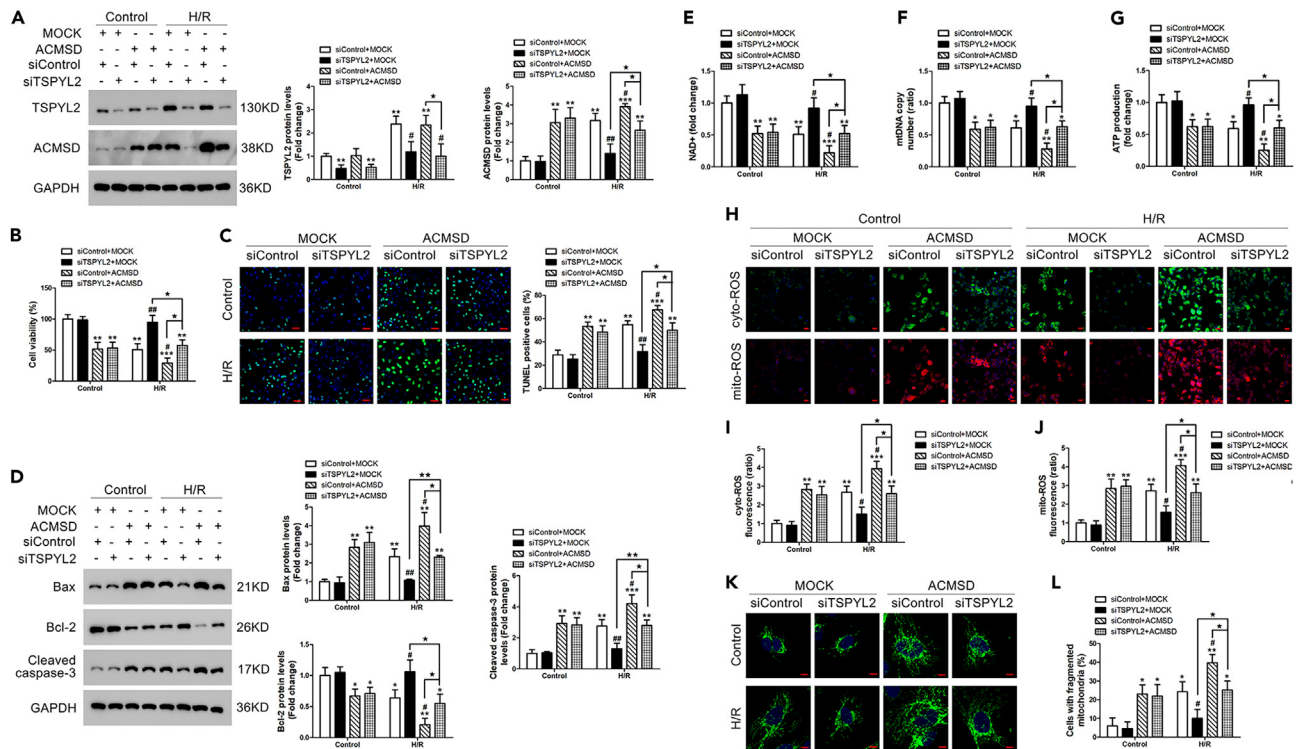
Figure 6. ACMSD overexpression aggravated mitochondrial dysfunction, oxidative stress and apoptosis induced by H/R injury in TSPYL2-knockdown HK-2 cells

(A) HK-2 cells were transfected with siTSPYL2 or siControl and a plasmid carrying the human ACMSD or the mock plasmid without ACMSD 24 h before exposure to H/R or no exposure (Control). Representative Western blots show the protein expression of TSPYL2 and ACMSD in HK-2 cells and the bar graph shows the quantification of blots from three independent experiments.

(B) Cell viability was measured using the CCK8 kit in HK-2 cells in the indicated groups.

(C) Apoptosis in HK-2 cells was detected by TUNEL assay. Bar = 50 μm. The bar graph shows the percentage of TUNEL apoptotic cells.

(D) Representative Western blots of the protein expression of Bax, Bcl-2, and cleaved caspase-3 in HK-2 cells are shown. GAPDH was a loading control. Bar graphs show the results of protein levels of Bax, Bcl-2, and cleaved caspase-3 in HK-2 cells from three independent experiments.

(E) NAD^+ levels in HK-2 cells were measured.

(F) mtDNA copy number in HK-2 cells was determined by analysis of the ND1 segment-18S segment ratio using qPCR.

(G) Cellular ATP production was measured in HK-2 cells.

(H–J) Staining of cytoplasmic ROS (cyto-ROS) in green and mitochondrial ROS (mito-ROS) in red in HK-2 cells was performed using CellROX green reagent and MitoSOX red reagent, respectively. Bar = 20 μm. Bar graphs showing relative fluorescence levels of cyto-ROS (I) and mito-ROS (J) are shown.

(K) Representative images of mitochondrial divisions in HK-2 cells are shown by the immunohistochemical staining of mitochondria in green. Bar = 5 μm.

(L) Mitochondrial fission was quantified in HK-2 cells by counting the percentage of cells with fragmented mitochondria. Data are represented as mean ± SD. p value calculated was determined by a two-tailed unpaired Student's t test. *, #, ★ p < 0.05, **, ##, ★★ p < 0.01; * versus Control-siControl+MOCK group; # versus the H/R-siControl+MOCK group.

Interestingly, compared to the H/R-treated siTSPYL2 cells the p300 levels were increased in H/R-treated siTSPYL2+siSIRT1 cells (Figure 7I), suggesting that TSPYL2 may regulate the p300 activity via SIRT1. These data suggests that TSPYL2 regulates SREBP-2 acetylation by reducing SIRT1 and increasing p300 protein levels.

DISCUSSION

Renal IRI causes loss of kidney function and cell damage of the proximal tubule structure, which eventually leads to AKI. Unfortunately, the molecular mechanisms involved in renal IRI following disrupted renal flow are not exactly clear. We hypothesized that the TSPYL2 may be a regulator of apoptosis in the kidneys after IRI as it was demonstrated that TSPYL2 stimulates cell death upon DNA damage[15] and is related to TGF-β-mediated fibrogenesis as well as diabetes-associated renal injury.[22] Therefore, we investigated the role of TSPYL2 in renal IRI using a mouse IRI model and a cell H/R model. Findings of the two models were consistent and showed that TSPYL2 is upregulated upon IRI in mice and H/R injury in the cell line. The pivotal role of TSPYL2 in IRI in the kidneys was demonstrated by reduced kidney injury, apoptosis, and oxidative stress after IRI or H/R injury in knockdown experiments of TSPYL2.
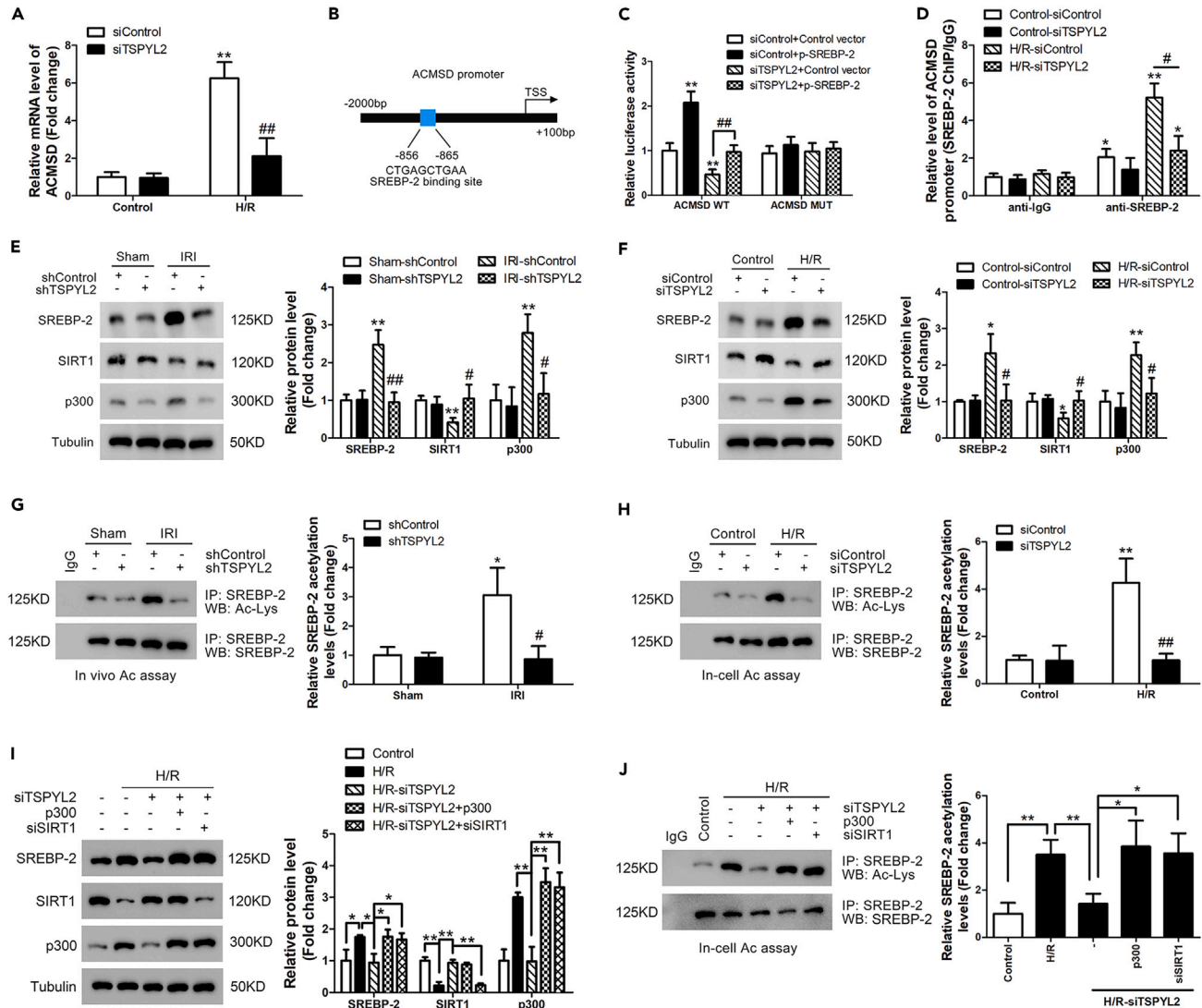
Figure 7. TSPYL2 promotes ACMSD transcriptional activation by regulating SREBP-2 acetylation

(A) HK-2 cells were transfected with siTSPYL2 or siControl for 24 h before exposure to H/R or no exposure (Control). The mRNA level of ACMSD was determined for the four groups. **p < 0.01 versus Control-siControl group; ##p < 0.01 versus the H/R-siControl group.

(B) A predicted binding sites of SREBP-2 to the ACMSD promoter was found when searching the JASPAR database. Base pair (bp) numbers indicate positions relative to the ACMSD transcription start site (TSS). The blue box indicates the SREBP-2-binding motif.

(C) HK-2 cells were transfected with siTSPYL2 or siControl and Control vector or a plasmid carrying SREBP-2 (p-SREBP-2). Luciferase reporter analysis was performed 24h later based on the wild-type and mutant ACMSD promoter regions expressed in HK-2 cells. **p < 0.01 versus ACMSD WT-siControl+Control vector group.

(D) HK-2 cells were transfected with siTSPYL2 or siControl and exposed to H/R after 24h or not exposed (Control). Thereafter, cells were collected for ChIP assays to detect the binding of SREBP-2 at the ACMSD promoter. Pull-down was performed with anti-IgG or anti-SREBP-2 antibodies. Levels of ACMSD promoter were measured in samples and normalized to the levels of the IgG pull-down assay in the Control-siControl group. *p < 0.05, **p < 0.01 versus anti-IgG-Control-siControl group.

(E) The protein expression of SREBP-2, SIRT1, and p300 in the kidneys of sham-treated mice and IRI-exposed mice earlier injected with shControl or shTSPYL2 was analyzed by Western blotting. Representative blots are shown and bar graphs of the quantitative analyses of several experiments. **p < 0.01 versus Sham-shControl group; #p < 0.05 versus IRI-shControl group.

(F) HK-2 cells were transfected with siTSPYL2 or siControl. Cells were exposed to H/R after 24h or not exposed (Control). Protein levels of SREBP-2, SIRT1, and p300 were detected by Western blotting. Representative blots are shown and bar graphs of the quantitative analyses of several experiments. **p < 0.01 versus Control-siControl group; #p < 0.05 versus the H/R-siControl group.

(G) Endogenous SREBP-2 was immunoprecipitated from mouse kidney tissues of sham-treated mice or IRI-exposed mice which were earlier injected with shControl or shTSPYL2. In immunoprecipitates, acetylated SREBP-2 was detected by Western blotting. Staining for SREBP-2 was done to check for the

Figure 7. Continued

immunoprecipitation of SREBP-2. Quantification of band of acetylated and total SREBP-2 were performed and acetylated SREBP-1 levels relative to total levels were calculated and normalized to the value of sham-shControl mice. *p < 0.05 versus Sham-shControl group; #p < 0.05 versus IRI-shControl group.

(H) Endogenous SREBP-2 was immunoprecipitated from HK-2 cells exposed to H/R or not exposed (Control) which were earlier transfected with siTSPYL2 or siControl. Acetylated SREBP-2 was detected by Western blotting in immunoprecipitates. SREBP-2 acetylation was detected by Western blotting by incubating with acetyl-Lys antibody. Staining for SREBP-2 was done to check for the immunoprecipitation of SREBP-2. Quantification of band of acetylated and total SREBP-2 were performed and acetylated SREBP-1 levels relative to total levels were calculated and normalized to the value of Control-cells. **p < 0.01 versus Control-siControl group; ##p < 0.01 versus the H/R-siControl group.

(I) HK-2 cells were transfected with siTSPYL2 in combination with a plasmid carrying p300 or siSIRT1. After 24h, cells were exposed to H/R or not exposed (Control). Protein levels of SREBP-2, SIRT1, and p300 were detected by Western blotting. Representative blots are shown and bar graphs of the quantitative analyses of three experiments. *p < 0.05, **p < 0.01.

(J) HK-2 cells were transfected with siTSPYL2 in combination with a plasmid carrying p300 or siSIRT1. After 24h, cells were exposed to H/R or not exposed (Control). Endogenous SREBP-2 was immunoprecipitated and acetylated SREBP-2 was detected by Western blotting. A bar graph shows the results of the SREBP-2 acetylation/total SREBP-2 ratio in HK-2 cells which is normalized to the value of Control cells. *p < 0.05, **p < 0.01. Data are represented as mean ± SD. p value calculated was determined by a two-tailed unpaired Student's t test.

NAD+ is a cosubstrate for several enzymes, including the sirtuin family of NAD+-dependent protein deacylases. Increased levels of NAD+ and activation of sirtuin have beneficial effects on mitochondrial hemostasis, implicating that NAD+ is an important player for renal health. Recently, ACMSD has been identified as a tissue-selective key checkpoint of the *de novo* NAD+ synthesis pathway across species.[21] ACMSD expression was found to be enriched in the kidney and liver, suggesting that the regulation of ACMSD and NAD+ levels could be an interesting target for therapeutic interventions for disease compromising hepatic and renal function, such as AKI. Indeed, the inhibition of ACMSD with a chemical compound in an animal model of AKI induced by ischemia-reperfusion showed increased NAD+ content and protection from structural and functional renal damage caused by IRI.[21] In our study, we confirmed the increased ACMSD levels in the mouse IRI model and in the cell H/R model with reduced. Moreover, we preformed experiments with the knockdown and overexpression of ACMSD and demonstrated the important role of ACMSD following IRI in inducing kidney dysfunction and cell damage.

In search for the regulator of ACMSD expression, we found that the promotor region of ACMD has an SREBP-2 binding site and by ChIP analysis of HK-2 cells we demonstrated that upon H/R injury, TSPYL2 mediated SREBP-2 binding to the promoter of ACMSD. Moreover, luciferase reporter analysis showed that SREBP-2 indeed transactivate the ACMSD promoter and eliminate the inhibition effect of TSPYL2 knockdown. Our results indicate that TSPYL2 regulates the ACMSD promoter activity via SREBP-2 binding. Studies on the link between SREBP-2 and ACMSD are limited to one study by Matsuda et al.,[23] who suggested that in rat hepatocytes *ACMSD* gene expression was subjected to sterol-dependent regulation and may be upregulated by SREBP-2.

Interestingly, in the study of Katsyuba et al., the inhibition of ACMSD in HK-2 cells resulted in the upregulation of transcription of mitochondrial and ROS defense genes in a SIRT1-dependent manner.[21] These results indicate that SIRT1 is involved in the pathway of IRI leading to the activation of ACMSD and regulation of NAD+ content. A previous study identified TSPYL2 as a novel regulator of SIRT1 inhibition and promotion of p300 acetylation and activation in response to DNA damage.[18] Our findings demonstrated the regulation of SIRT1 and p300 by TSPYL2 in response to IRI in the kidney. Furthermore, our cotransfection experiments suggested that TSPYL2 regulates SREBP-2 acetylation by inhibiting SIRT1 and promoting p300 activity after IRI. Interestingly, knockdown of SIRT1 upregulated the p300 levels in - TSPYL2-knockdown cells after H/R, suggesting that TSPYL2 may regulate the p300 activity via SIRT1. Binding of SREBP to p300 was earlier suggested in a search for potential coactivators of SREBP.[24] The investigators of this study found that the putative activation domain of SREBP bound specifically to amino-terminal domains of recombinant CREB-binding proteins (CBP) and the CBP-relation protein p300. With regard to SIRT1, a study by Li and Wu suggested a pathway in hepatocytes that involved the targeting of SREBP-2 through SIRT1 signaling, indicating a link between these two proteins.[25] Other studies have demonstrated that the deacetylation of SREBP-1/2 by SIRT1 destabilizes SREBP-1/2.[26,27] It was found that SIRT1 can directly deacetylate SREBP, and SIRT1 may thereby play an important role in the regulation of SREBP-dependent gene regulation. These earlier findings are consistent with our findings on the negative regulation of SREBP by SIRT1.

Limitations of the study

TSPYL2 has been found to have an induction role for p53 regulation and p53-dependent apoptosis by inhibiting SIRT1 and promoting p300 activity in human DNA-damaged cells. It should be interesting to investigate the role of p53 regulated by TSPYL2, which may be involved in apoptosis and in stress response in IRI. But the role of p53 regulated by TSPYL2 has not been confirmed in AKI, which may be a limitation of the study. p53, as a well-known tumor suppressor, is involve in AKI and subsequent kidney repair via regulating several cell biologic processes, such as cell-cycle arrest and apoptosis.[28] However, the pathogenic role of p53 in AKI remains controversial. A study indicated that proximal tubule p53 knockout mice were resistant to ischemic and cisplatin nephrotoxic AKI, whereas other tubular p53 knockout mice were sensitive to AKI, implying that p53 may have cell type-specific roles in AKI.[29] Therefore, further studies would be performed to investigate the complicated role of p53 regulated by TSPYL2 in AKI.

After IRI, the pathological process is controlled by complex signaling pathways, involving in the interaction of multiple genes and regulation in signal pathways, such as p53, WNT/β-catenin signaling and transforming growth factor β (TGF-β) signaling.[30,31] Most studies suggested that TGF-β is an injurious factor and inhibition of TGF-β signaling pathway may reduce acute renal tubular injury.[32–34] In mice with diabetic nephropathy, the genetic deletion of TSPYL2, the gene encoding CDA1, reduced the TGF-β signaling. In epithelial tissues, the

TSPYL2 complex with REST enhances TGF-β signaling by repressing the expression of genes, reduced the such as the proto-oncogene neurotrophic tyrosine kinase receptor C (TrkC).[35] These results indicated TSPYL2 is an import regulator for TGF-β signaling pathway, which may mediate renal injury regulated by TSPYL2. However, more research is required to confirm the interaction of TSPYL2 and other signal pathways in AKI, which contributes to better understand the implication role of TSPYL2 in renal ischemia-reperfusion injury.

STAR★METHODS

Detailed methods are provided in the online version of this paper and include the following:

- KEY RESOURCES TABLE
- RESOURCE AVAILABILITY
  - Lead contact
  - Materials availability
  - Data and code availability
- EXPERIMENTAL MODEL AND STUDY PARTICIPANT DETAILS
  - Animals and renal IRI model
  - Cell culture and cell hypoxia/reoxygenation (H/R) model
- METHOD DETAILS
  - Plasmid construction and injection/transfection
  - Evaluation of renal function
  - Histological examination
  - Immunofluorescent staining
  - Quantitative real-time PCR
  - Western blot analysis
  - TUNEL assays
  - Determination of ROS levels
  - NAD + and NADH measurement
  - Measurement of adenosine triphosphate (ATP) levels
  - Cell viability
  - Measurement of MDA, SOD, and GSH
  - Luciferase reporter assay
  - Chromatin immunoprecipitation (ChIP) assay
  - In-cell and *in vivo* acetylation assays
- QUANTIFICATION AND STATISTICAL ANALYSIS

SUPPLEMENTAL INFORMATION

Supplemental information can be found online at https://doi.org/10.1016/j.isci.2024.109594.

AUTHOR CONTRIBUTIONS

Z.L and Z.W conceived the project and designed the research and revised the article. S.M, Y.S, Z.P, L.Yhong, and C.K designed and performed the experiments, analyzed and interpreted the data and wrote the article. L.Yhua, L.H, and L.Yf performed and analyzed *in vitro* experiments. All authors read and approved the final article.

DECLARATION OF INTERESTS

The authors declare no competing interests.

REFERENCES

1. Hoste, E.A.J., Bagshaw, S.M., Bellomo, R., Cely, C.M., Colman, R., Cruz, D.N., Edipidis, K., Forni, L.G., Gomersall, C.D., Govil, D., et al. (2015). Epidemiology of acute kidney injury in critically ill patients: the multinational AKI-EPI study. Intensive Care Med. *41*, 1411–1423. https://doi.org/10.1007/s00134-015-3934-7.

2. Ronco, C., Bellomo, R., and Kellum, J.A. (2019). Acute kidney injury. Lancet *394*, 1949–1964. https://doi.org/10.1016/S0140-6736(19)32563-2.

3. Brown, J.R., Rezaee, M.E., Marshall, E.J., and Matheny, M.E. (2016). Hospital Mortality in the United States following Acute Kidney Injury. BioMed Res. Int. *2016*, 4278579. https://doi.org/10.1155/2016/4278579.

4. Kashani, K., Rosner, M.H., Haase, M., Lewington, A.J.P., O'Donoghue, D.J., Wilson, F.P., Nadim, M.K., Silver, S.A., Zarbock, A., Ostermann, M., et al. (2019). Quality Improvement Goals for Acute Kidney Injury. Clin. J. Am. Soc. Nephrol. *14*, 941–953. https://doi.org/10.2215/CJN.01250119.

5. Zuk, A., and Bonventre, J.V. (2019). Recent advances in acute kidney injury and its consequences and impact on chronic kidney disease. Curr. Opin. Nephrol. Hypertens. *28*, 397–405. https://doi.org/10.1097/MNH.0000000000000504.

6. Bonventre, J.V., and Yang, L. (2011). Cellular pathophysiology of ischemic acute kidney injury. J. Clin. Invest. *121*, 4210–4221. https://doi.org/10.1172/JCI45161.

7. Funk, J.A., and Schnellmann, R.G. (2012). Persistent disruption of mitochondrial homeostasis after acute kidney injury. Am. J. Physiol. Ren. Physiol. *302*, F853–F864. https://doi.org/10.1152/ajprenal.00035.2011.

8. Zsengellér, Z.K., Ellezian, L., Brown, D., Horváth, B., Mukhopadhyay, P., Kalyanaraman, B., Parikh, S.M., Karumanchi, S.A., Stillman, I.E., and Pacher, P. (2012). Cisplatin nephrotoxicity involves mitochondrial injury with impaired tubular mitochondrial enzyme activity. J. Histochem. Cytochem. *60*, 521–529. https://doi.org/10.1369/0022155412446227.

9. Zhang, Q., Raoof, M., Chen, Y., Sumi, Y., Sursal, T., Junger, W., Brohi, K., Itagaki, K., and Hauser, C.J. (2010). Circulating mitochondrial DAMPs cause inflammatory responses to injury. Nature *464*, 104–107. https://doi.org/10.1038/nature08780.

10. Bonventre, J.V., and Weinberg, J.M. (2003). Recent advances in the pathophysiology of ischemic acute renal failure. J. Am. Soc. Nephrol. *14*, 2199–2210. https://doi.org/10.1097/01.asn.0000079781.13922.f6.

11. Che, R., Yuan, Y., Huang, S., and Zhang, A. (2014). Mitochondrial dysfunction in the pathophysiology of renal diseases. Am. J. Physiol. Ren. Physiol. *306*, F367–F378. https://doi.org/10.1152/ajprenal.00571.2013.

12. Kribben, A., Edelstein, C.L., and Schrier, R.W. (1999). Pathophysiology of acute renal failure. J. Nephrol. *12*, S142–S151.

13. Wang, G.S., Hong, C.J., Yen, T.Y., Huang, H.Y., Ou, Y., Huang, T.N., Jung, W.G., Kuo, T.Y., Sheng, M., Wang, T.F., and Hsueh, Y.P. (2004). Transcriptional modification by a CASK-interacting nucleosome assembly protein. Neuron *42*, 113–128. https://doi.org/10.1016/s0896-6273(04)00139-4.

14. Li, Y., and Lau, Y.F.C. (2008). TSPY and its X-encoded homologue interact with cyclin B but exert contrasting functions on cyclin-dependent kinase 1 activities. Oncogene *27*, 6141–6150. https://doi.org/10.1038/onc.2008.206.

15. Tao, K.P., Fong, S.W., Lu, Z., Ching, Y.P., Chan, K.W., and Chan, S.Y. (2011). TSPYL2 is important for G1 checkpoint maintenance upon DNA damage. PLoS One *6*, e21602. https://doi.org/10.1371/journal.pone.0021602.

16. Garaycoechea, J.I., Quinlan, C., and Luijsterburg, M.S. (2023). Pathological consequences of DNA damage in the kidney. Nat. Rev. Nephrol. *19*, 229–243. https://doi.org/10.1038/s41581-022-00671-z.

17. Molitoris, B.A. (2019). DNA damage response protects against progressive kidney disease. J. Clin. Invest. *129*, 4574–4575. https://doi.org/10.1172/JCI131171.

18. Magni, M., Buscemi, G., Maita, L., Peng, L., Chan, S.Y., Montecucco, A., Delia, D., and Zannini, L. (2019). TSPYL2 is a novel regulator of SIRT1 and p300 activity in response to DNA damage. Cell Death Differ. *26*, 918–931. https://doi.org/10.1038/s41418-018-0168-6.

19. Chai, Z., Dai, A., Tu, Y., Li, J., Wu, T., Wang, Y., Hale, L.J., Koentgen, F., Thomas, M.C., and Cooper, M.E. (2013). Genetic deletion of cell division autoantigen 1 retards diabetes-associated renal injury. J. Am. Soc. Nephrol. *24*, 1782–1792. https://doi.org/10.1681/ASN.2013010060.

20. Ralto, K.M., Rhee, E.P., and Parikh, S.M. (2020). NAD(+) homeostasis in renal health and disease. Nat. Rev. Nephrol. *16*, 99–111. https://doi.org/10.1038/s41581-019-0216-6.

21. Katsyuba, E., Mottis, A., Zietak, M., De Franco, F., van der Velpen, V., Gariani, K., Ryu, D., Cialabrini, L., Matilainen, O., Liscio, P., et al. (2018). De novo NAD(+) synthesis enhances mitochondrial function and improves health. Nature *563*, 354–359. https://doi.org/10.1038/s41586-018-0645-6.

22. Chen, L., Wu, J., Hu, B., Liu, C., and Wang, H. (2021). The Role of Cell Division Autoantigen 1 (CDA1) in Renal Fibrosis of Diabetic Nephropathy. BioMed Res. Int. *2021*, 6651075. https://doi.org/10.1155/2021/6651075.

23. Matsuda, H., Sato, M., Yakushiji, M., Koshiguchi, M., Hirai, S., and Egashira, Y. (2014). Regulation of rat hepatic alpha-amino-beta-carboxymuconate-epsilon-semialdehyde decarboxylase, a key enzyme in the tryptophan- NAD pathway, by dietary cholesterol and sterol regulatory element-binding protein-2. Eur. J. Nutr. *53*, 469–477. https://doi.org/10.1007/s00394-013-0547-1.

24. Oliner, J.D., Andresen, J.M., Hansen, S.K., Zhou, S., and Tjian, R. (1996). SREBP transcriptional activity is mediated through an interaction with the CREB-binding protein. Genes Dev. *10*, 2903–2911. https://doi.org/10.1101/gad.10.22.2903.

25. Li, Y., and Wu, S. (2018). Epigallocatechin gallate suppresses hepatic cholesterol synthesis by targeting SREBP-2 through SIRT1/FOXO1 signaling pathway. Mol. Cell. Biochem. *448*, 175–185. https://doi.org/10.1007/s11010-018-3324-x.

26. Ponugoti, B., Kim, D.H., Xiao, Z., Smith, Z., Miao, J., Zang, M., Wu, S.Y., Chiang, C.M., Veenstra, T.D., and Kemper, J.K. (2010). SIRT1 deacetylates and inhibits SREBP-1C activity in regulation of hepatic lipid metabolism. J. Biol. Chem. *285*, 33959–33970. https://doi.org/10.1074/jbc.M110.122978.

27. Walker, A.K., Yang, F., Jiang, K., Ji, J.Y., Watts, J.L., Purushotham, A., Boss, O., Hirsch, M.L., Ribich, S., Smith, J.J., et al. (2010). Conserved role of SIRT1 orthologs in fasting-dependent inhibition of the lipid/cholesterol regulator SREBP. Genes Dev. *24*, 1403–1417. https://doi.org/10.1101/gad.1901210.

28. Tang, C., Ma, Z., Zhu, J., Liu, Z., Liu, Y., Liu, Y., Cai, J., and Dong, Z. (2019). P53 in kidney injury and repair: Mechanism and therapeutic potentials. Pharmacol. Ther. *195*, 5–12. https://doi.org/10.1016/j.pharmthera.2018.10.013.

29. Zhang, D., Liu, Y., Wei, Q., Huo, Y., Liu, K., Liu, F., and Dong, Z. (2014). Tubular p53 regulates multiple genes to mediate AKI. J. Am. Soc. Nephrol. *25*, 2278–2289. https://doi.org/10.1681/ASN.2013080902.

30. Overstreet, J.M., Gifford, C.C., Tang, J., Higgins, P.J., and Samarakoon, R. (2022). Emerging role of tumor suppressor p53 in acute and chronic kidney diseases. Cell. Mol. Life Sci. *79*, 474. https://doi.org/10.1007/s00018-022-04505-w.

31. He, L., Wei, Q., Liu, J., Yi, M., Liu, Y., Liu, H., Sun, L., Peng, Y., Liu, F., Venkatachalam, M.A., and Dong, Z. (2017). AKI on CKD: heightened injury, suppressed repair, and the underlying mechanisms. Kidney Int. *92*, 1071–1083. https://doi.org/10.1016/j.kint.2017.06.030.

32. Chung, S., Overstreet, J.M., Li, Y., Wang, Y., Niu, A., Wang, S., Fan, X., Sasaki, K., Jin, G.N., Khodo, S.N., et al. (2018). TGF-beta promotes fibrosis after severe acute kidney injury by enhancing renal macrophage infiltration. JCI Insight *3*, e123563. https://doi.org/10.1172/jci.insight.123563.

33. Gewin, L., Vadivelu, S., Neelisetty, S., Srichai, M.B., Paueksakon, P., Pozzi, A., Harris, R.C., and Zent, R. (2012). Deleting the TGF-beta receptor attenuates acute proximal tubule injury. J. Am. Soc. Nephrol. *23*, 2001–2011. https://doi.org/10.1681/ASN.2012020139.

34. Shang, J., Sun, S., Zhang, L., Hao, F., and Zhang, D. (2020). miR-211 alleviates ischaemia/reperfusion-induced kidney injury by targeting TGFbetaR2/TGF-beta/SMAD3 pathway. Bioengineered *11*, 547–557. https://doi.org/10.1080/21655979.2020.1765501.

35. Epping, M.T., Lunardi, A., Nachmani, D., Castillo-Martin, M., Thin, T.H., Cordon-Cardo, C., and Pandolfi, P.P. (2015). TSPYL2 is an essential component of the REST/NRSF transcriptional complex for TGFbeta signaling activation. Cell Death Differ. *22*, 1353–1362. https://doi.org/10.1038/cdd.2014.226.

36. Sui, M., Xu, D., Zhao, W., Lu, H., Chen, R., Duan, Y., Li, Y., Zhu, Y., Zhang, L., and Zeng, L. (2021). CIRBP promotes ferroptosis by interacting with ELAVL1 and activating ferritinophagy during renal ischaemia-reperfusion injury. J. Cell Mol. Med. *25*, 6203–6216. https://doi.org/10.1111/jcmm.16567.

37. Liu, H., Wang, L., Weng, X., Chen, H., Du, Y., Diao, C., Chen, Z., and Liu, X. (2019). Inhibition of Brd4 alleviates renal ischemia/reperfusion injury-induced apoptosis and endoplasmic reticulum stress by blocking FoxO4-mediated oxidative stress. Redox Biol. *24*, 101195. https://doi.org/10.1016/j.redox.2019.101195.

38. Chen, S., Fu, H., Wu, S., Zhu, W., Liao, J., Hong, X., Miao, J., Luo, C., Wang, Y., Hou, F.F., et al. (2019). Tenascin-C protects against acute kidney injury by recruiting Wnt ligands.

Kidney Int. *95*, 62–74. https://doi.org/10.1016/j.kint.2018.08.029.

39. Jablonski, P., Howden, B.O., Rae, D.A., Birrell, C.S., Marshall, V.C., and Tange, J. (1983). An experimental model for assessment of renal recovery from warm ischemia. Transplantation *35*, 198–204. https://doi.org/10.1097/00007890-198303000-00002.

40. Wang, J., Zhu, P., Li, R., Ren, J., Zhang, Y., and Zhou, H. (2020). Bax inhibitor 1 preserves mitochondrial homeostasis in acute kidney injury through promoting mitochondrial retention of PHB2. Theranostics *10*, 384–397. https://doi.org/10.7150/thno.40098.

41. Cai, C., Zhang, Y., and Peng, X. (2021). Knocking down Sterol regulatory element binding protein 2 (SREBF2) inhibits the Serine Protease 8 (PRSS8)/sodium channel epithelial 1alpha subunit (SCNN1A) axis to reduce the cell proliferation, migration and epithelial-mesenchymal transformation of ovarian cancer. Bioengineered *12*, 9390–9400. https://doi.org/10.1080/21655979.2021.1978615.

STAR★METHODS

KEY RESOURCES TABLE

REAGENT or RESOURCE	SOURCE	IDENTIFIER
Antibodies		
Rabbit polyclonal anti-TSPYL2	This paper	N/A
Rabbit polyclonal anti-ACMSD	Invitrogen	Cat# PA5-21790, RRID:AB_11155616
Rabbit monoclonal cleaved Caspase-3	Cell Signaling Technology	Cat# 9664, RRID:AB_2070042
Mouse monoclonal anti-Bax	Santa Cruz Biotechnology	Cat# sc-20067, RRID:AB_626726
Mouse monoclonal anti-Bcl-2	Santa Cruz Biotechnology	Cat# sc-7382, RRID:AB_626736
Mouse monoclonal anti-SREBP-2	Santa Cruz Biotechnology	Cat# sc-271615, RRID:AB_10709730
Mouse monoclonal anti-Acetylated-Lysine (Ac-Lys)	Cell Signaling Technology	Cat# 9441, RRID:AB_331805
Mouse monoclonal anti-SIRT1	Santa Cruz Biotechnology	Cat# sc-74465, RRID:AB_1129462
Mouse monoclonal anti-p300	Santa Cruz Biotechnology	Cat# sc-48343, RRID:AB_628075
Mouse monoclonal anti-GAPDH	Santa Cruz Biotechnology	Cat# sc-365062, RRID:AB_10847862
Mouse monoclonal anti-Tubulin	Abcam	Cat# ab44928, RRID:AB_2241150
HRP-labeled Goat anti-Rabbit IgG (H + L)	Beyotime	Cat# A0208, RRID:AB_2892644
HRP-labeled goat anti-mouse IgG (H + L)	Beyotime	Cat# A0216, RRID:AB_2860575
Rabbit polyclonal anti-TOMM20	Abcam	Cat# ab186735, RRID:AB_2889972
Chemicals, peptides, and recombinant proteins		
CellROX™ Green Reagent	Invitrogen	Cat# C10444,
MitoSOX red mitochondrial superoxide indicator	Invitrogen	Cat# M36008
trichostatin A	Sigma-Aldrich	Cat# V900931
nicotinamide	Sigma-Aldrich,	Cat# N0636
Critical commercial assays		
Mouse KIM-1 Immunoassay Quantikine® ELISA	R&D Systems	Cat# MKM100
PrimeScript™ RT Reagent Kit	TaKaRa Biotech	Cat# DRR037A
SYBR® Premix Ex TaqTM kit	TaKaRa Biotech	Cat# DRR041A
TIANAMP Genomic DNA Extraction Kit	TIANGEN	Cat# 4992199
TUNEL assay kit	Thermo Fisher Scientific, Inc.	Cat# C10618
ROS assay kit	Solarbio	Cat# CA1410
NAD/NADH Assay Kit	Abcam	Cat# ab65348
luciferin-luciferase assay kit	Beyotime	Cat# S0026
CCK-8 assay	Beyotime	Cat# C0038
Lipid Peroxidation (MDA) Assay Kit	Abcam	Cat# ab118970
Glutathione Assay Kit	Jiancheng Biotech	Cat# A006-1-1
Superoxide dismutase (SOD) Assay Kit	Jiancheng Biotech	Cat# A001-3
ChIP assay kit	Millipore	Cat# 17-10086
Experimental models: Cell lines		
Human HK-2 cells: hypoxia/reoxygenation (H/R) model	Liu et al.[37]	N/A
Experimental models: Organisms/strains		
C57BL/6J mice: renal IRI model	Sui et al.[36]	N/A
Oligonucleotides		
TSPYL2 shRNA sequence: CACCGGAAGATGCTCATGAC CATTATTCAAGAGATAATGGTCATGAGCATCTTCCTTTTTT	This paper	N/A

Continued

REAGENT or RESOURCE	SOURCE	IDENTIFIER
Control shRNA sequence: CACCGTTCGACTCACGTGTC ACGTTCAAGAGACGTGACACGTGAGTCGAACTTTTTT	This paper	N/A
siRNA targeting sequences: human TSPYL2 #1–3, see Table S1	This paper	N/A
siRNA targeting sequences: human ACMSD #1–3, see Table S1	This paper	N/A
siRNA targeting sequences: human SIRT1 #1–3, see Table S1	This paper	N/A
siRNA targeting sequences: non-specific negative control, see Table S1	This paper	N/A
Primer for qPCR, see Table S2	This paper	N/A
Recombinant DNA		
Plasmid: pGPU6/GFP/Neo	GenePharma Co. Ltd.	Cat# E−07
Plasmid: pGPU6-shTSPYL2	This paper	N/A
Plasmid: pGPU6-shControl	This paper	N/A
Plasmid: pcDNA3.1- ACMSD	This paper	N/A
Plasmid: pcDNA3.1- SREBP-2	This paper	N/A
Plasmid: pcDNA3.1- p300	This paper	N/A
Plasmid: pGL3-ACMSD promoter-WT	This paper	N/A
Plasmid: pGL3-ACMSD promoter-MUT	This paper	N/A
Plasmid: pRL-CMV	Promega	E2261
Software and algorithms		
ImageJ software	National Institutes of Health (NIH)	https://imagej.nih.gov/ij/
Other		
Olympus FV1000 Confocal Microscope	Olympus	RRID:SCR_020337
SpectraMax M5 Multimode Plate Reader	Molecular Devices	RRID:SCR_020300

RESOURCE AVAILABILITY

Lead contact

Further information and requests for resources and reagents should be directed to and will be fulfilled by the lead contact, Li Zeng (shchyysyz@smmu.edu.cn).

Materials availability

This study did not generate new unique reagents.

Data and code availability

All data reported in this paper will be shared by the lead contact upon request.

This paper does not report original code.

Any additional information required to reanalyze the data reported in this paper is available from the lead contact upon request.

EXPERIMENTAL MODEL AND STUDY PARTICIPANT DETAILS

Animals and renal IRI model

Eight-week-old male C57BL/6J mice (25–30 g, n = 6 per group) were obtained from the Research Center of Medical Experimental Animals of Shanghai Changhai Hospital, Naval Medical University (Shanghai, China). The protocol of animal experiments was approved by the Shanghai Changhai Hospital Ethics Committee [the permission number: CHEC(A.E)2023-010], Naval Medical University, and all procedures complied with the Guide for Care and Use of Laboratory Animals of Shanghai Changhai Hospital. The renal IRI model in mice was established as previously described.[36] In brief, the renal pedicles were clamped for 30 min followed by removal of the clamp to allow reperfusion of the kidney. During inducing ischemic, mice body temperature was keeping up at 32°C using a heat-pad. Reperfusion was allowed to continue for 6, 12 or 24 h. In the Sham group, mice were operated with the identical surgical procedures except that the clamps were not applied and they were killed at 24h after surgery. Mice were sacrificed at the appointed time after IRI, and blood and tissue samples were collected.

Cell culture and cell hypoxia/reoxygenation (H/R) model

As previously described,[37] HK-2 (human renal proximal tubular epithelial) cells were kept in DMEM culture medium with addition of nonessential amino acids, 0.05 mg/mL, bovine pituitary extract, 50 ng/mL, human recombinant epidermal growth factor, 100 U/mL, penicillin, 100 μg/mL streptomycin, and 10% fetal bovine serum. Cells were cultured under conditions of 5% CO_2 and 95% air atmosphere at 37°C.

To establish the cell H/R model, HK-2 cells were cultured for 12 h under hypoxic conditions (1% O_2, 94% N_2 and 5% CO_2) in DMEM medium without nutrients. After cells were exposed to hypoxic injury, medium was refreshed and cells were moved to a normoxic cell incubator (5% CO_2 and 95% air) for 2, 4 and 6 h for reoxygenation.

METHOD DETAILS

Plasmid construction and injection/transfection

For knockdown and overexpression of *in vivo* protein expression in mice, an shRNA-mediated approach was used. An shRNA expression vector containing TSPYL2 shRNA was constructed using pGPU6/GFP/*Neo* (GenePharma Co. Ltd., Shanghai, China) and for the negative control, the shRNA was randomly scrambled (shControl). Briefly, mouse TSPYL2 or control shRNA was inserted into the plasmid at the BbsI/BamHI site. The following oligonucleotides of the TSPYL2 shRNA were: 5′-CACCGGAAGATGCTCATGACCATTATTCAAGAGATAATGGTCAT GAGCATCTTCCTTTTTT -3′, 5′- GATCAAAAAAGGAAGATGCTCATGACCATTATTCAAGAGATAATGGTCATGAGCATCTTCC-3′. The following oligonucleotides of the control shRNA were: 5′-CACCGTTCGACTCACGTGTCACGTTCAAGAGACGTGACACGTGAGTC GAACTTTTTT -3′, 5′- GATCAAAAAAGTTCGACTCACGTGTCACGTTCAAGAGACGTGACACGTGAGTCGAAC -3′. Mice were injected with 20μg shRNA plasmids diluted in 1.8 mL saline in the tail vein using the hydrodynamic-based gene delivery technique, as previously described.[38] Two days later, mice were exposed to IRI or underwent the same surgery without clamping renal vessels (sham). Animals were sacrificed 24 h after IRI.

For *in vitro* knockdown of proteins in the cell model, small interfering RNAs (siRNAs) targeting human TSPYL2 (siTSPYL2), human ACMSD (siACMSD) or human SIRT1 (siSIRT1) and non-specific negative control oligos (siNC) were obtained from Gene Pharma Co. Ltd. (Shanghai, China). The siRNA targeting sequences were shown in Table S1. For *in vitro* overexpression of aminocarboxymuconate-semialdehyde decarboxylase (ACMSD), SREBP-2 or p300, the full-length cDNA of human ACMSD, SREBP-2 or p300 was inserted into pcDNA3.1 and the mock plasmid without ACMSD, SREBP-2 or p300 cDNA was used as the negative control. HK-2 cells were seeded into a 6-well plate. At a cell density of 70%–80%, cells were transfected with the oligos or plasmid using the Lipofectamine 3000 reagent. Two days after transfection, the transfection efficiency was examined by Western blotting.

Evaluation of renal function

Levels of serum creatinine and blood urea nitrogen (BUN) were determined by an automatic chemistry analyzer and expressed as milligrams per deciliter. Kidney injury molecule-1 (KIM-1) was measured in mouse urine samples by ELISA (R&D Systems).

Histological examination

Hematoxylin and eosin (H&E) staining of sections was performed as follows. Sections of fixed and embedded kidneys of mice were gradually deparaffinized, hydrated and stained with H&E. Morphological assessment was performed by observers who used an established grading scale of 0–4 for the histopathological assessment of IRI-induced damage.[39]

Immunofluorescent staining

Tissue sections of frozen mouse kidneys were fixed with 4% formaldehyde and permeabilized with 0.2% Triton X-100 for 5 min. Samples were rinsed three times with PBS, blocked with 10% goat serum for 1 h and incubated with the primary antibodies overnight at 4°C. The following antibodies were used: anti-TSPYL2 (Beijing Biosynthesis Biotechnology Co. Ltd), anti-cleaved caspase-3 (Cell Signaling Technology, Danvers, MA, USA), anti-ACMSD (Invitrogen), and the mitochondrial marker Tom20 (1:250, ab186735, Abcam, RRID:AB_2889972). After washing, the cells were incubated with fluorescent-labeled secondary antibodies for 1h at 37°C. DAPI (Sigma, St. Louis, MO, USA) was used for staining of cell nuclei. Images were captured by a confocal microscope (Olympus FV1000, Tokyo, Japan, RRID:SCR_020337). Mitochondrial fission was evaluated by cell counts of fragmented mitochondria. Immunofluorescence was measured by converting immunosignals into average fluorescence intensity, which was analyzed using ImageJ software (National Institutes of Health, NIH).

Quantitative real-time PCR

From kidney samples or HK-2 cells, total RNA was isolated using TRIzol reagent (Thermo Fisher Scientific) according to the manufacturer's instructions. The isolated RNA was reverse transcribed into cDNA using a PrimeScript RT Reagent Kit (TaKaRa Biotech, Dalian, China). Total genomic DNA was extracted from HK-2 cells using the TIANAMP Genomic DNA Extraction Kit (TIANGEN) according to the manufacturer's instructions. The mtDNA copy number was determined by qPCR analysis using specific primers for the mtDNA marker ND1 gene and normalized to the expression of the nuclear intron of 18S RNA (nDNA marker). The level of mtDNA copy number was represented as the mtDNA/nDNA ratio. Quantitative real-time PCR analysis was performed using the SYBR Premix Ex TaqTM kit (Takara) and an ABI PRISM 7900 Sequence Detection system (Life Technologies, Grand Island, NY, USA). GAPDH mRNA expression was used as an internal control. Relative expression levels of the genes were calculated using the $2^{-\Delta\Delta Ct}$ method. The qPCR primers are shown in Table S2.

Western blot analysis

Protein expression was analyzed by Western blotting as previously described.[37] In short, renal tissues and HK-2 cells were lysed and protein samples were separated on SDS polyacrylamide gels and transferred to PVDF membranes. Membranes were blocked with milk and incubated with primary antibodies. The following antibodies were used: anti-TSPYL2 (1:500, bs-7051R, Beijing Biosynthesis Biotechnology Co. Ltd); anti-ACMSD (1:1000, PA5-21790, Invitrogen; RRID:AB_11155616); anti-cleaved Caspase-3 (1:1000, #9664, Cell Signaling Technology, Danvers, MA, USA; RRID:AB_2070042); anti-Bax (1:200, sc-20067, Santa Cruz Biotechnology, Santa Cruz, CA, USA; RRID:AB_626726); anti-Bcl-2 (1:200, sc-7382; Santa Cruz Biotechnology; RRID:AB_626736); anti-SREBP-2 (1:100, sc-271615, Santa Cruz Biotechnology; RRID:AB_10709730); anti-Acetylated-Lysine (Ac-Lys) (1:1000, #9441, Cell Signaling Technology; RRID:AB_331805); anti-SIRT1 (1:100, sc-74465, Santa Cruz Biotechnology; RRID:AB_1129462); anti-p300 (1:100, sc-48343, Santa Cruz Biotechnology; RRID:AB_628075); anti-GAPDH (1:100, sc-365062, Santa Cruz Biotechnology; RRID:AB_10847862) and anti-Tubulin (1:100, ab44928, Abcam; RRID:AB_2241150). After incubation with secondary antibodies, bands were visualized by chemiluminescent HRP substrate. ImageJ software was used for quantification of protein levels.

TUNEL assays

Apoptotic in the paraffin-embedded mouse kidney sections and HK-2 cells was performed using a TUNEL assay kit (Thermo Fisher Scientific, Inc.) according to the manufacturer's instructions, as previously described.[40]

Determination of ROS levels

To measure the cellular ROS levels in sections of mouse kidney tissues, flow cytometry was performed. In brief, fresh mouse kidney tissue was cut into 1 mm parts and samples were centrifuged twice for 2 min (4°C, 1500 rpm). After centrifugation, the supernatant was discarded. Subsequently, the solution was digested by adding trypsin (0.25%) at room temperature for 5 min, and digestion was terminated by the addition of serum. Then, the solution was filtered through a 70 μm filter and 5 to 10 mL PBS was used to rinse the sample. The filtrate was collected and centrifuged twice (5 min, 4°C, 1500 rpm). The pellet after centrifugation consisted of kidney cells. Cellular ROS levels were analyzed by flow cytometry after staining the cells using a ROS assay kit (ROS, CA1410, Solarbio).

To stain for mitochondrial ROS (mito-ROS) and cytoplasmic ROS (cyto-ROS) in cells, MitoSOX red mitochondrial superoxide indicator (M36008) and CellROX Green Reagent (C10444, both from Invitrogen, Inc.) were used. For quantification, the fluorescent signals were converted into average grayscale intensities, which were subsequently analyzed using ImageJ software.

NAD + and NADH measurement

Quantification of NAD^+ and NADH levels was carried out using the NAD/NADH Assay Kit (Abcam) according to the manufacturer's instructions. NAD^+ and NADH values were normalized to kidney cortex wet weight.

Measurement of adenosine triphosphate (ATP) levels

The intracellular ATP level was measured using a luciferin-luciferase assay kit (Beyotime, China) according to the manufacturer's instructions. Briefly, 40 μL of cell extracts or ATP standard reaction solution, ranging from 100 nM to 5 μM, was added to 96-well luminescence assay plates. Then, 100 μL of reaction buffer was added to each well. Luminescence was measured by a fluorescence microplate reader (Thermo Fisher Scientific) at 562 nm absorbance. The cellular ATP content was calculated according to the ATP standard curve.

Cell viability

Cell viability was assessed using the CCK-8 assay (Beyotime, China) according to the manufacturer's instructions. Briefly, HK-2 cells were seeded into 96-well plates at a density of 5×10^3 cells/well. After overnight culture, the cells were transfected with siRNA and/or expression plasmids for 24h before exposure to H/R injury. After H/R exposure, cells were incubated with CCK-8 reagent. Then, cell viability was assessed by absorbance measurements at 450 nm using a SpectraMax M5 microplate reader (Molecular Devices, San Jose, CA, USA, RRID:SCR_020300).

Measurement of MDA, SOD, and GSH

Lipid peroxidation levels in cell and tissue lysates were determined by measuring malondialdehyde (MDA) levels with the Lipid Peroxidation (MDA) Assay Kit (Abcam). Glutathione (GSH) was measured in cell and tissue lysates using the Glutathione Assay Kit and superoxide dismutase (SOD) activity levels were measured using a commercial kit (Jiancheng Biotech, Nanjing, China), all used according to manufacturer's instructions. Samples were measured using a spectrophotometer (SpectraMax M5, Molecular Devices, USA, RRID:SCR_020300).

Luciferase reporter assay

HK-2 cells were transfected with plasmids with SREBP-2 or a control vector plus the luciferase reporter plasmids containing the wild-type ACMSD promoter region (ACMSD WT) or the mutated ACMSD promoter region (ACMSD MUT) using Lipofectamine TM 2000 reagent (Invitrogen, Waltham, MA, USA). The cells were collected 24 h after transfection and analyzed using a dual luciferase reporter assay system

(Promega, Madison, WI, USA). Luciferase activity was normalized to Renilla luciferase activity, and relative luciferase activity was reported as fold induction over the controls after normalizing for transfection efficiency.

Chromatin immunoprecipitation (ChIP) assay

The chromatin immunoprecipitation (ChIP) assay was performed as previously described.[41] In short, the ChIP assay kit (Millipore, Darmstadt, Germany) was used according to the instructions provided. 90% Of the chromatin was diluted in ChIP dilatation buffer and incubated with 5 μL anti- SREBP-2 antibody or normal immunoglobulin (IgG). The remainder 10% was kept as the input control. Expression was detected by RT-qPCR. ChIP data were shown as the percentage of the input normalized to control purifications.

In-cell and *in vivo* acetylation assays

For in-cell assay, HK-2 cells in 6-well plates were co-transfected with siTSPYL2, and siSIRT1, or the expression plasmids for p300. To inhibit deacetylase activity, cells were treated with the deacetylase inhibitors trichostatin A (500 nM, Sigma-Aldrich, V900931) and freshly prepared nicotinamide (Nam; 10 Mm, Sigma-Aldrich, N0636) for 2–5 h before preparing cell extracts.

For *in vivo* acetylation assay, nuclear extracts of the kidney were obtained in the presence of deacetylase inhibitors. Endogenous SREBP-2 was immunoprecipitated at 4°C for 2 h in immunoprecipitation buffer and washed four times with immunoprecipitation buffer. Acetylated SREBP-2 levels were detected by Western blotting using Acetylated-Lysine antibody.

QUANTIFICATION AND STATISTICAL ANALYSIS

The results are shown as mean $\pm$ standard deviation (SD). Differences were tested using the two-tailed unpaired Student's t test. $p < 0.05$ (*, #, ★) or $p < 0.01$ (**, ##, ★★) indicates a statistically significant difference. All of the statistical details of experiments can be found in the figure legends.